Nordic Steel Construction Conference 2015
Tampere, Finland
23-25 September 2015

BUCKLING OBSERVATION OF DOOR OPENINGS FOR WIND TURBINE TOWERS

Anh Tuan Tran[a], Milan Veljkovic[a], Carlos Rebelo[b], Luis Simoes da Silva[b]

[a] Luleå University of Technology, Sweden
anhtuan.tran@ltu.se, milan.veljkovic@ltu.se
[b] University of Coimbra, ISISE, Portugal
crebelo@dec.uc.pt, luisss@dec.uc.pt

Abstract: This paper presents experimental and FE results of buckling study around door openings for steel tubular wind turbine towers. Compression tests, using circular and polygonal down scale specimens with and without openings, have been performed in the approximately scale 1:10. A software package has been used to compare and analyse the images in order to gain insight into the local buckling development. Finite element analyses of the numerical models have been also performed and results have been compared with test results.

1 Introduction

Tower is an important part of the wind turbine support structure. The tower transfers wind loading from rotor and self-weight load of whole structure to the foundation. Most of the current wind turbine towers have circular cross sections. However, the polygonal cross sections are also considered in the towers design.

Door opening is essential part of the wind turbine tower. It is a dispensable part and used to maintain operation of the wind turbine. However, the door opening is a weak point of the tower on structural aspect. Buckling of the wind turbine tower may occur around the door opening. Several studies focusing on buckling of the door opening are presented in previous papers [1-3].

To get a better understanding on the development of the buckling around opening, experimental and FE investigations were performed. In these investigations, compression tests of the down-scale specimens were carried out with an Aramis system [7]. The Aramis system observed the development of the buckling during the compression tests in real time. FE analyses of the compression tests are also implemented by Abaqus software [5]. Results from the experiments and the FE analyses are presented in this paper.

2 Experimental programme

2.1 Test specimens and preparation

There were four specimens taken into the study. They included one circular specimen without opening, one circular specimen with opening, one polygonal specimen without opening and one polygonal specimen with opening. All specimens have 1000 mm length and 4 mm plate thickness. The widths of the polygonal specimens and the circular specimens are 305 mm and 307 mm respectively, Fig 1 and Fig 2.

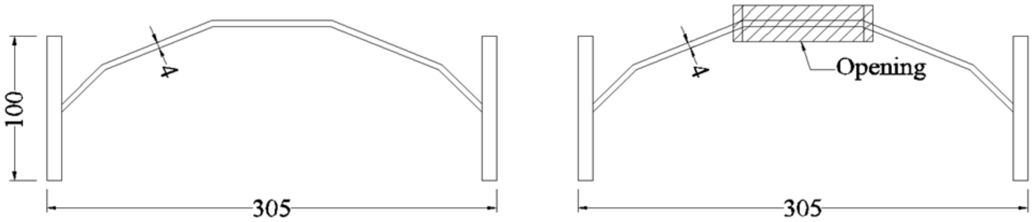

Fig. 1: a) Polygonal specimen without opening; b) Polygonal specimen with opening.

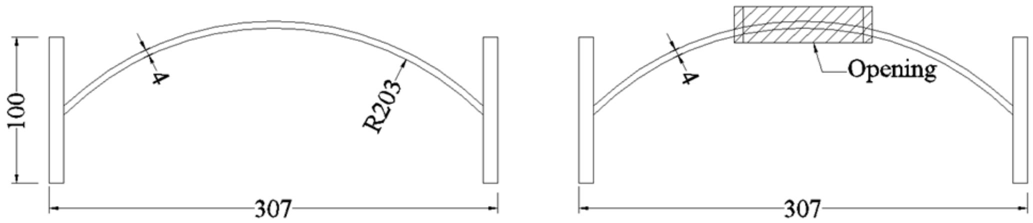

Fig. 2: a) Circular specimen without opening; b) Circular specimen with opening.

Geometric imperfections influence significantly on the buckling shapes of the specimens. Therefore, geometric imperfections were measured carefully in all specimens. First, the surfaces of specimens were prepared and target points were glued. Target points were used to help the laser scanner to measure geometric imperfection, Fig 3. Second, 3D laser scanner was used to measure the geometric imperfections. The scanner was moved over the surfaces of the specimens. The right distance between specimen and the equipment is controlled by the signal of the scanner. Geometric imperfections were analysed by Gom Inspect software [6]. The detail of the 3D laser scanning measurement was presented in [4].

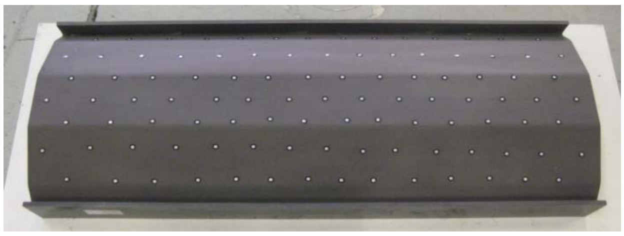

Fig. 3: Preparation of specimen surface for scanning geometric imperfections [4].

In order to observe buckling development during the compression test, a non-contact optical 3D deformation measuring system (Aramis system) was used. For using this method, the observed areas of specimens need to be prepared. The areas were painted with contrast colour in order to help the Aramis system to record images. For these specimens, black and white colours were used. Most importance is the size and number of pattern dot and number of dot in a facet. Diameters of pattern-dot used are around 3 pixel and 3-4 dots in one Facet. The observed areas were determined from the tested specimens. For the specimens with opening, the observed areas are around opening. For the specimens without opening, the observed areas are around the top of the specimens. Figure 4 shows preparation of the specimen surface for buckling observation.

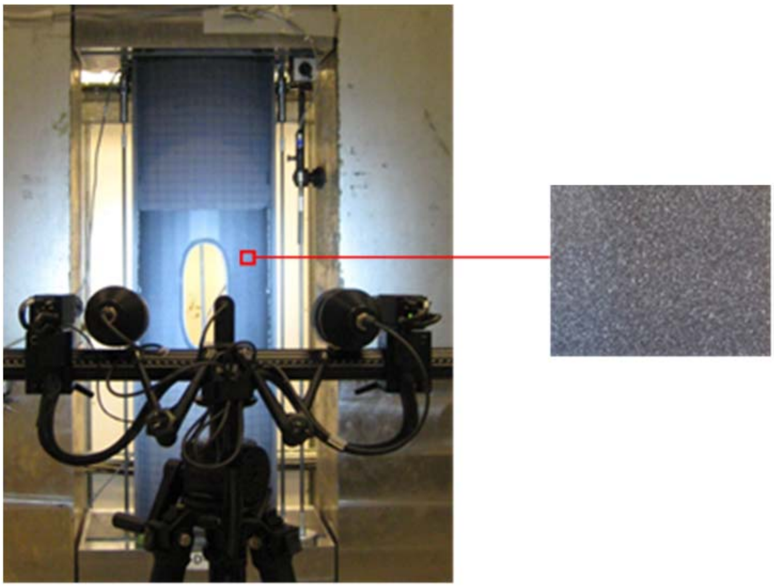

Fig. 4: Preparation of specimen surface for buckling observation.

2.2 Buckling observation during compression tests

During the compression tests, Aramis system records, compares and calculates digital images in order to obtain displacements and deformation of the specimens. The non-contact optical 3D deformation measuring system used is ARAMIS and PONTOS 2D/3D with Sensor Controller. The packet of system includes two cameras, stand, sensor controller, calibration cross 700 CC 20/MV 700x560 mm2 and ARAMIS software v6.3 [7]. The images are recorded by 2 cameras. The camera angle to measured surface is about 25 degree. Figure 5 shows set-up of compression tests with the Aramis system.

Fig. 5: Set-up compression tests with Aramis system.

Figure 6 shows the typical set-up of the compression tests. The Instron system with a capacity of 4500 kN was used for the compression tests. Four LVDTs were used to measure displacements of the specimens. Displacement control was applied for all the compression tests. Speed of displacement was 0.001 mm/s. It would be emphasized that material of the specimens is high strength steel S650. Therefore, on the top and bottom of the specimens were attached high strength steel plates Ramor 500. The steel plates were used in order to avoid the thrust of the specimens into steel blocks. Before the compression tests, centre lines of the specimens and the compression machine were checked by laser equipment.

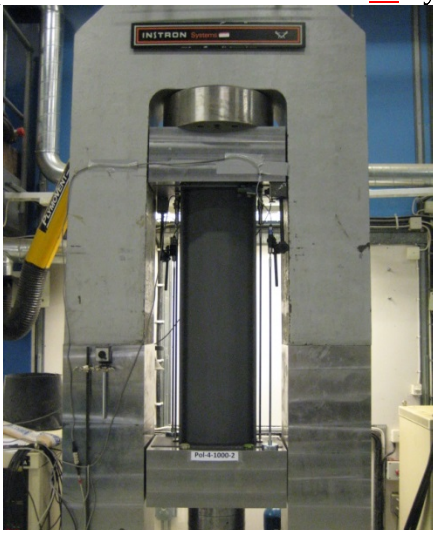

Fig. 6: Typical compression test set-up.

3 Finite element models

The finite element analysis program Abaqus was used to analyse the numeric models of the compression tests. In abaqus, there are some different shell elements types that can be used: STRI3(S) (3-node triangular facet thin shell), S3 (shell element with 3 nodes and full numerical integration), S4 (shell element with 4 nodes and full numerical integration), S4R (shell element with 4 nodes and reduced numerical integration), S8R (shell element with 8 nodes and reduced numerical integration). For these models, shell elements S4R were used. Because, the S4R elements are suitable for larger strain of buckling and riks analysis.

Material used was high strength steel grade S650. In order to investigate material characteristic, coupon specimens were machined off from flat part, corner part and circular part of the specimens. Data from tensile tests were considered as material input data for the numerical models. Geometric imperfections from 3D laser scanning tests were used to create the shape of the numerical models.

Boundary conditions were applied as follows: fixed all translation and rotation on bottom, fixed all translation and rotation except direction of applied load on top.
Figure 7 shows the mesh of the numerical models without opening and with the opening. Refinement of FE mesh was especially considered in order to have nodes appropriate for implementation of geometric imperfections.

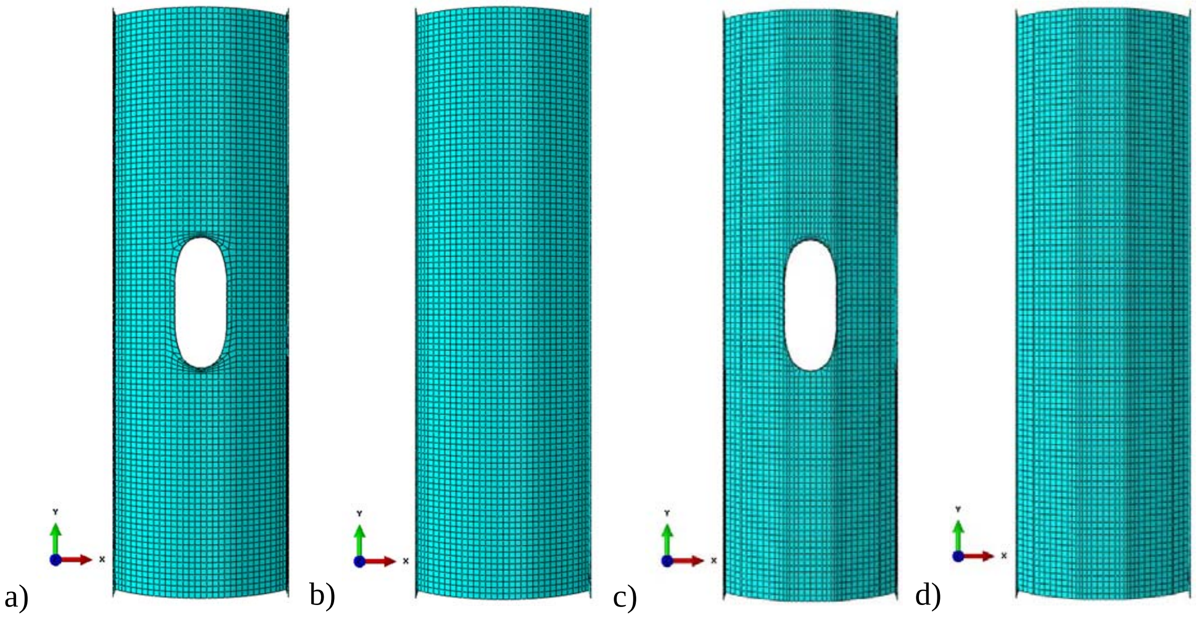

Fig. 7: a) circular model with opening; b) circular model without opening; c) polygonal model with opening and d) polygonal model without opening.

4 Results and discussion

4.1 Buckling analysis

Figure 8 shows the first buckling modes of the numerical models. Buckling of both the circular and the polygonal models with opening occurs at the door openings. Minimum deformation in U3 direction of the polygonal model with opening is smaller approximate 45% than the circular model with opening. Whereas, U3 deformation of the polygonal model without opening is higher about 17% than the circular model without opening. Buckling characteristic of the circular model without opening is local buckling waves. They occur on the top of the model. Buckling of the polygonal model without opening appears in the plate between corners.

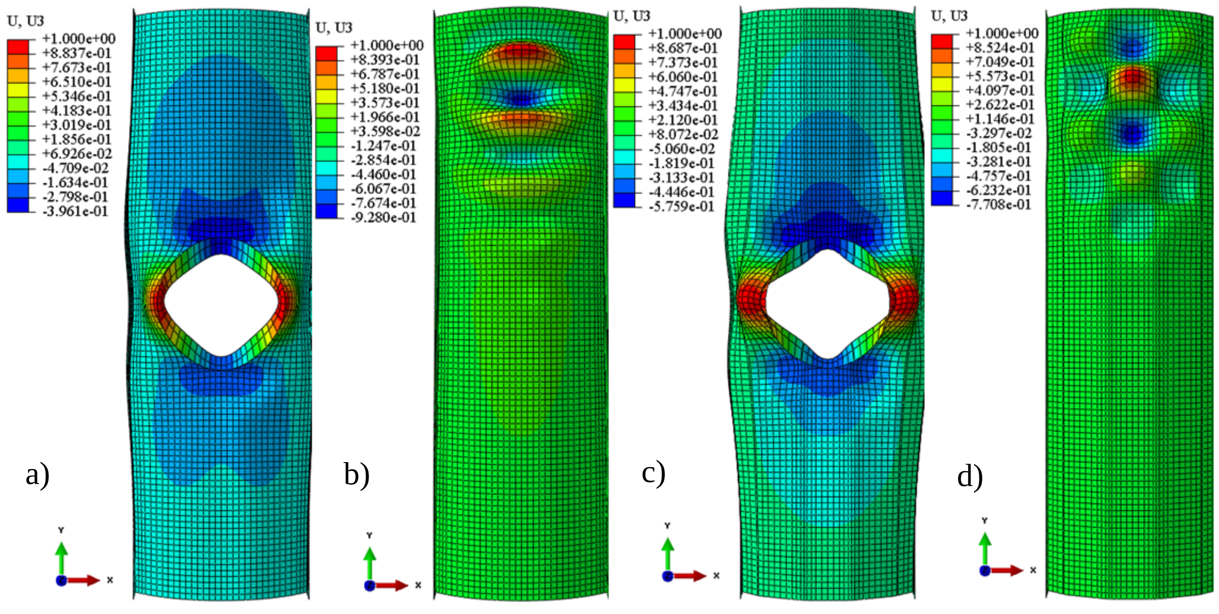

Fig. 8: First buckling mode of a) circular model with opening; b) circular model without opening; c) polygonal model with opening and d) polygonal model without opening.

Comparison of first three modes between the models is presented in Table 1. It would be interesting to emphasize that eigenvalues of the circular model with opening are bigger than the polygonal model with opening. It reaches maximum 10.74% bigger at the buckling mode 2. The eigenvalue of the circular model without opening is also significantly higher than the polygonal model without opening. It is 27.15% higher at the buckling mode 1. The comparison also reflects considerable influence of the door opening on the eigenvalues of the models.

Table 1: Comparison of first three eigenvalues between models.

	Circular model with opening	Circular model without opening	Polygonal model with opening	Polygonal model without opening
Mode 1	1.000	1.556	0.977	1.223
Mode 2	1.145	1.564	1.034	1.234
Mode 3	1.181	1.643	1.079	1.340

Table 2 presents comparison of the critical loads between the models. The openings significantly influence on the critical loads. The critical loads of the circular models and polygonal models are considerably influenced by the opening, decreasing 35.7% and 20.1% respectively. It must be emphasized that the cross section area and length of circular and polygonal models are similar. The difference of the cross section areas is just 0.3%. However, the critical load of the circular model without opening is bigger 26.7% than the polygonal model without opening.

Table 2: Comparison of critical loads between models.

	Circular model without opening	Circular model with opening	Polygonal model without opening	Polygonal model with opening
Critical load (kN)	5772	3709	4557	3643

4.2 Buckling development

The buckling development around opening of the polygonal specimen with opening is presented in Fig 9. Positive deformations in U3 direction occur at two side of the opening. Negative U3 deformations appear on the top and bottom of the opening. Maximum and minimum deformations reach 5.21 mm and -8.01 mm respectively at ultimate load applied. It is interesting to emphasize that the buckling around opening is asymmetrical. This asymmetry is caused by geometrical imperfections.

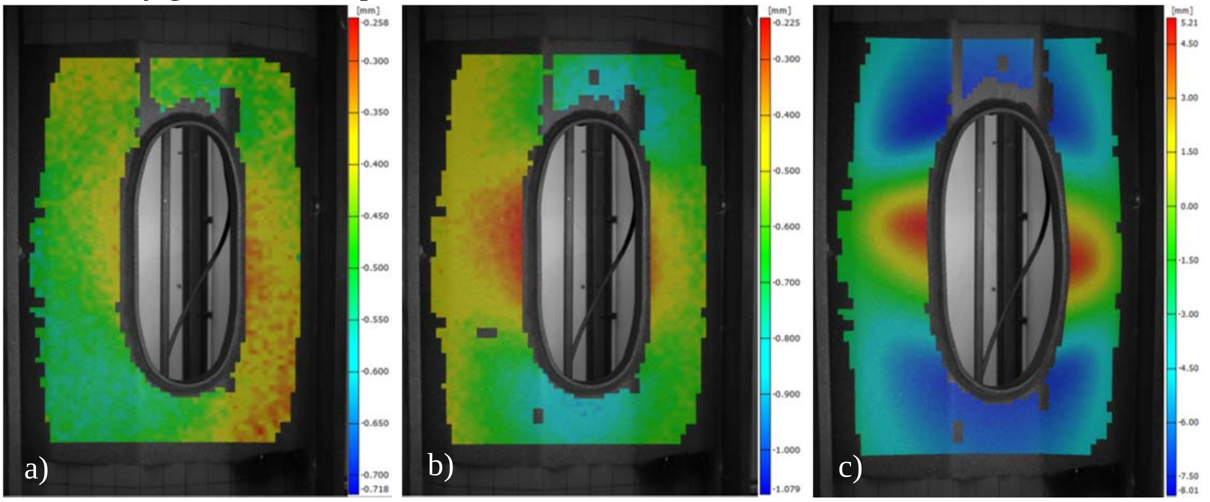

Fig. 9: Buckling development around opening of polygonal specimen with opening at applied load: a) 605.8 kN; b)1400.3 kN; c)1651.2 kN.

Figure 10 presents the buckling development around opening of the circular specimen with opening. First, the buckling occurs on the left side of the opening. Then the buckling spreads to the right side. However, the deformation on the right side is larger than on the left side. At the ultimate load, negative deformation transparently occurs on the left top and the right bottom of the opening.

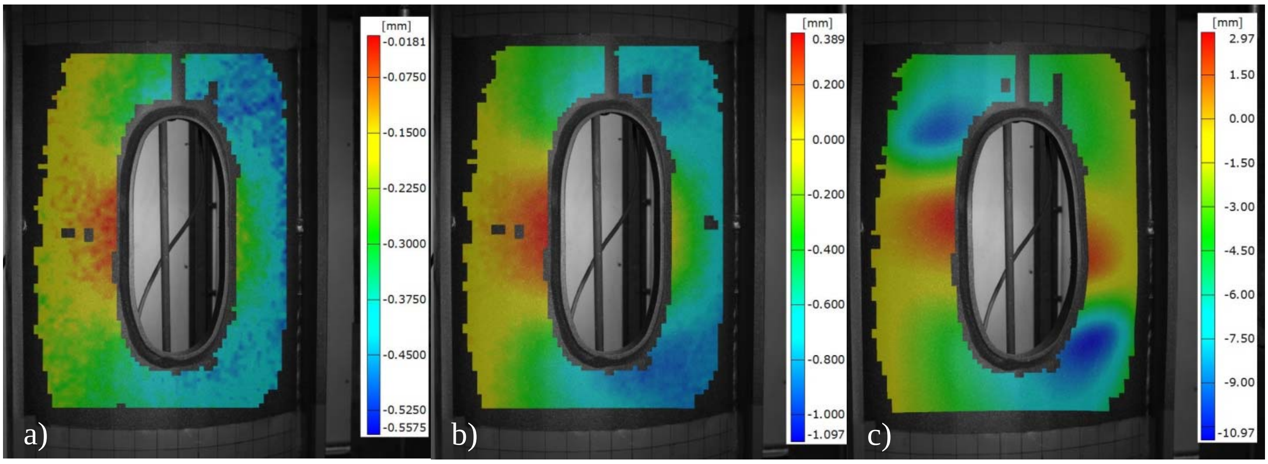

Fig. 10: Buckling development around opening of circular specimen with opening at applied load: a) 605.8 kN; b)1400.3 kN; c)1651.2 kN.

4.3 Nonlinear FE analysis

Geometrically and materially nonlinear analyses with imperfections (GMNIA) were developed in order to obtain the resistance of the numerical models. In abaqus [5], Riks method is used for the nonlinear analysis. This method solves the unstable response problem of structures. The initial increment in arc length λ_{in} needs to be provided at first step. For subsequent iterations and increments the value of arc length λ is to be computed automatically. The initial load proportionality factor l_{in} is calculated as follows:

$$\lambda_{in} = \frac{l_{in}}{l_{period}}$$

Where l_{period} is a user specified total arc length scale factor (typically equal to 1).

Figure 11 presents good agreement of buckling shape between FEA and experimental results. It would be emphasized that the applied load and the model are symmetrical. However, FEA result also specifies asymmetrical buckling around opening. It proves significant effect of geometric imperfections on the buckling shape.

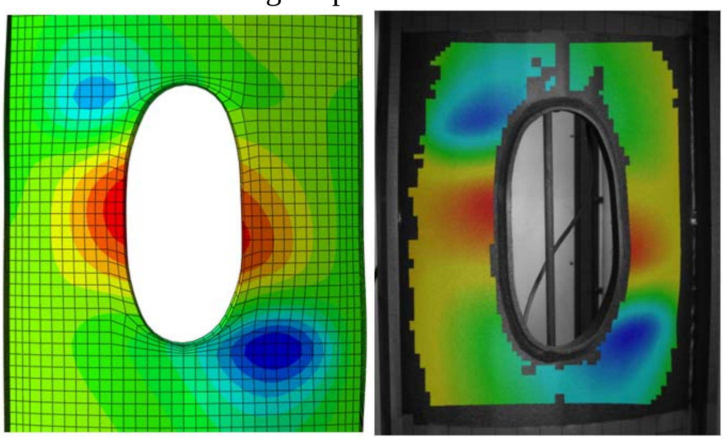

Fig. 11: Buckling around opening of the circular specimen with opening (FEA and experimental result).

5 Conclusions

The openings significantly influence on the critical loads. The critical loads of the circular models and polygonal models are considerably decreased by 35.7% and 20.1% respectively due to the presence of the opening. Critical loads of the circular models are higher than in the polygonal models. The critical load of the circular model without opening is 26.7% higher than the polygonal model without opening. Local buckling of door opening segment was successfully recorded in the experiment. Good agreement between compression experiments monitored by the system and FE results are obtained. Result of the buckling development calibrated to load – displacement curve is presented in Fig 12.

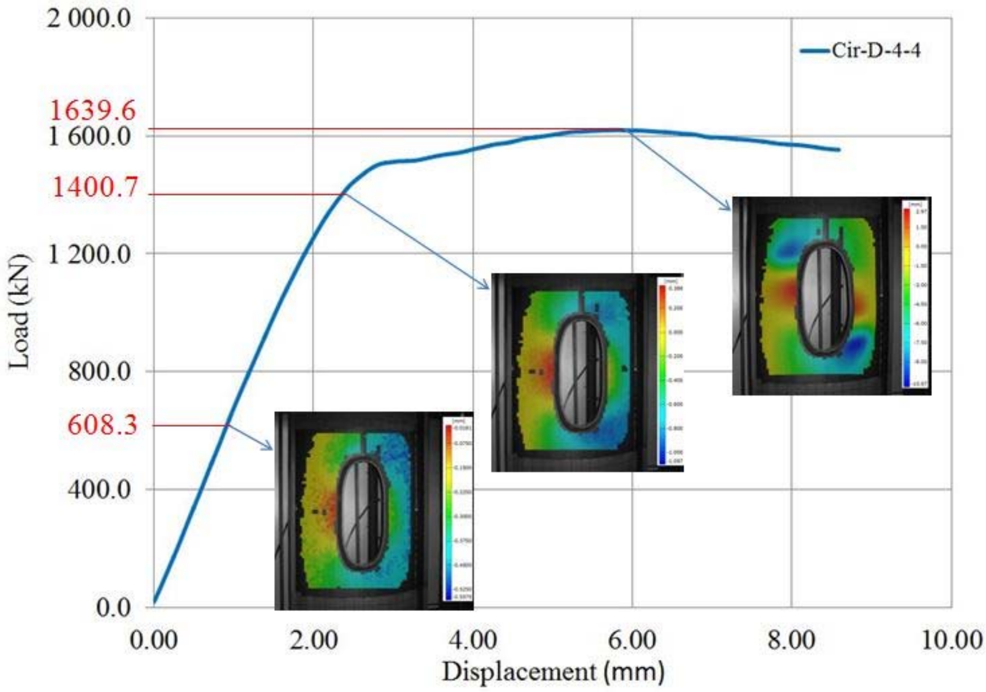

Fig. 12: Buckling development around opening.

Acknowledgements

The authors wish to thank the Research Fund for Coal and Steel for financially supporting the research in this paper through the Research Project HISTWIN 2.

References

[1] A.T. Tran, M. Veljkovic, C. Rebelo, L. Simões da Silva, *Resistance of door openings in towers for wind turbines*, 3rd South-East European Conference on Computational Mechanics an ECCOMAS and IACM Special Interest Conference, Kos Island, Greece, 2013.

[2] C.A. Dimopoulos, C.J. Gantes, *Experimental investigation of buckling of wind turbine tower cylindrical shells with opening and stiffening under bending*, Thin-Walled Structures, vol. **54**, pp. 140-155, 2012.

[3] J.F. Jullien, A. Limam, *Effects of openings of the buckling of cylindrical shells subjected to axial compression*, Thin-Walled Structures, vol. **31**, p. 187–202, 1998.

[4] Tran A.T, Veljkovic M, Rebelo C, L. Simões da Silva. *Influence of geometrical imperfections on analyses of door openings in tubular steel towers for wind turbines*. Proceeding of 7th European conference on Steel and Composite Structures, Napoli, Italy, 10-12 September 2014.

[5] Abaqus 6.12-1, Simulia Dassault Systmes, 2012.

[6] GOM Inspect V7.5, GOM mbH, 2013.

[7] ARAMIS software version 6.3, GOM mbH, 2013.